

See discussions, stats, and author profiles for this publication at: <https://www.researchgate.net/publication/306284611>

Mechanical behaviour of scaled-down unsupported tunnel walls in hard rock under high stress

Article in *Tunnelling and Underground Space Technology* · November 2016

DOI: 10.1016/j.tust.2016.07.012

CITATIONS

0

READS

58

3 authors:



Ayako Kusui

WA School of Mines - Curtin University

5 PUBLICATIONS 2 CITATIONS

SEE PROFILE



Ernesto Villaescusa

WA School of Mines - Curtin University Australia

135 PUBLICATIONS 471 CITATIONS

SEE PROFILE



Takahiro Funatsu

Curtin University

30 PUBLICATIONS 164 CITATIONS

SEE PROFILE

Mechanical Behaviour of Scaled-down Unsupported Tunnel Walls in Hard Rock under High Stress

A. Kusui, E. Villaescusa & T. Funatsu
WA School of Mines, CRC Mining, Curtin University

ABSTRACT

A large number of scaled-down tunnel experiments were undertaken to investigate the response of unsupported walls to an increased stress field. The experiments were undertaken in 200 mm diameter tunnels that were drilled into intact rock blocks of sandstone and granite ranging in strength from moderately strong to very strong. The tunnels were loaded by a servo-controlled, 450 tonne capacity INSTRON compression testing machine. As the ratio of intact rock strength to induced stress decreased, the unsupported tunnel walls became increasingly unstable. Critical ratios of compressive strength to induced stress were determined for critical instability stages such as tunnel spalling and also pillar crushing adjacent to the tunnels. The physical models have been simulated using three-dimensional finite element modelling. The values of the critical ratios correlate well with underground observations of full scale tunnels with similar Uniaxial Compressive Strength materials. Dynamic ejection velocities similar to those calculated from back analysis of actual failures have been determined. In addition, the seismic responses prior and during key failure stages have been established as a function of the increased loadings.

1. Introduction

As underground mining proceeds to depths below surface approaching or exceeding 1000m, the ratio of intact rock strength to induced stresses around conventional development excavations is such that failure of the rock mass adjacent to the excavations can occur very soon after construction. At the present time, such conditions have led to the abandonment of mining operations that have reached these depths, resulting in losses of hundreds of millions of dollars. In addition, over the next two decades or so, when the moderate depth resources are likely to be depleted, those conditions are likely to be faced routinely. Hence over the last three years the WA School of Mines (WASM) has undertaken a large number of laboratory experiments in order to understand the fundamentals of violent tunnel failure as a function of an increased induced stress.

The stability and behaviour of the rock masses surrounding an excavation are dependent upon several factors including the rock mass strength, the geometry of the excavation, the induced stresses surrounding the opening, the blasting or construction practices and the amount of water and weathering process (Hoek & Brown, 1980). In particular, the rock mass strength is a function of the intact rock properties and the geological discontinuities intersecting the rock mass near the

boundaries of an excavation. Furthermore, as mining progresses to greater depths, the induced stresses increase relative to the rock mass strength, such that excavation instability becomes increasingly apparent. Violent failures where the seismic source is located within the immediate vicinity of the excavation are often experienced (Figure 1).



Figure 1. Stress-driven failure near the boundary of an excavation.

Historically, the ratio of intact rock Uniaxial Compressive Strength (σ_c) to the induced compressive stress tangential to the wall of an excavation (σ_{max}) has been long recognized as a critical factor controlling excavation stability (Barton et al., 1974; Mathews et al., 1980). As the ratio of σ_c/σ_{max} reduces, excavation instability increases as shown in Figure 2. Data from many years of numerical modelling and observations of open stopping at Mount Isa Mines (Villaescusa, 2014) have shown that as the ratio decreases below the value of 5, the instability increases markedly. Large deformations are experienced in tunnels driven within low strength rock while sudden, violent failure occurs in tunnels excavated in high strength rock (Barla, 2014).

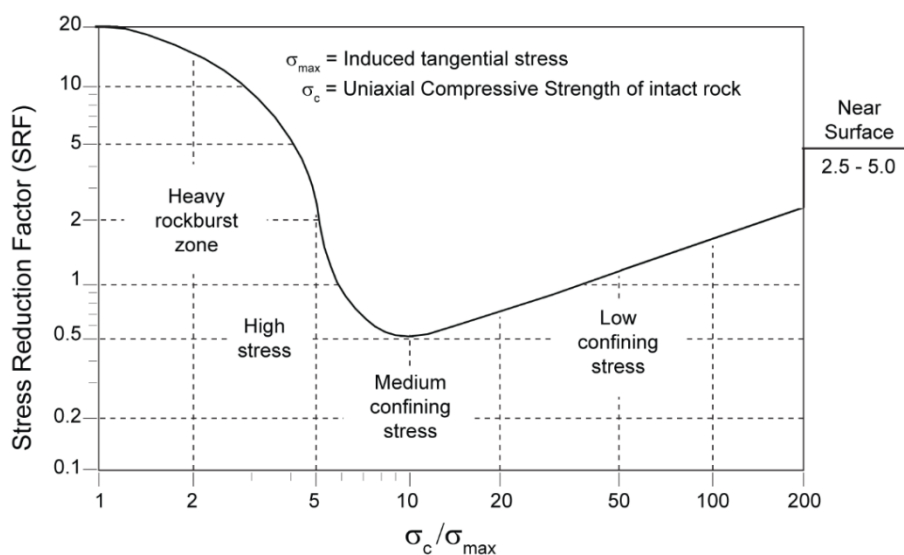


Figure 2. Excavation behaviour as a function of the ratio of compressive strength to the induced stress. (After Barton et al., 1974; Hutchinson and Diederichs, 1996)

2. Testing of Unsupported Scaled-down Tunnels

In order to investigate stress-driven fracturing around underground excavations, a large number of scaled-down tunnels have been constructed and tested at the WASM Rock Mechanics Laboratory.

2.1 Tunnel Models

The tunnels were constructed by drilling into 400W x 400H x 200D mm blocks of intact rock ranging in strength from moderately strong to very strong (20 to 200 MPa). The material consisted of soft and hard sandstone and also granite. The sandstone materials consisted of fine and coarse sand particles densely packed to form slightly coloured layers. The granite material consisted of quartz, feldspar and biotite. In all cases, the intact rock blocks were inspected and arranged such that the subsequent loading was undertaken perpendicular to any bedding or obvious geological weaknesses.

The size of the scaled down tunnels was in most cases 200mm in diameter, leaving 100 mm wide pillars both sides of the unsupported openings. However, in some experiments, 50mm and 100mm diameter tunnels were also constructed to compare the effects due to wider pillars adjacent to the simulated tunnels. Mechanical drilling of the miniature tunnels into the rock blocks minimised damage to the rock to ensure that any failure was predominantly stress-driven.

2.2 Test Configuration

The blocks of rock were constrained horizontally by two mild steel plates (16 mm thick) which were held by 4 threaded bars. This allowed the post-peak strength and behaviour to be determined during the tests. Prior to testing, the bolts were tightened with a known torque to apply small initial horizontal stresses on the side of the rock block.

The blocks of rock were loaded vertically using a 450 tonne capacity stiff INSTRON compression testing machine. The rate of loading was 0.5 mm/min.

Figure 3 shows a typical experimental set-up before and after testing. The depth of failure was largely controlled by the presence of geological discontinuities or potential planes of weakness.



Figure 3. Typical tunnel and pillar geometry tested (grid size 20 mm x 20 mm), before and after failure

2.3 Monitoring

Vertical load and vertical displacement were monitored during tests. Two acoustic emission sensors were installed to monitor the seismic response from initial loading to wall spalling and pillar crushing.

A high speed Canon EOS 650D video camera was used to monitor the tunnel walls during the progressive loading. This digital single-lens reflex camera, was set up in front of the sample and the tunnel behaviour was recorded through a special window within the INSTRON protective door. The camera is capable of capturing up to 50 frames per second. A set of special lights and a suitably placed background grid were used to estimate the displacement versus time motion of the failed particles that were ejected.

3. Computer Simulations

In order to better understand the failure processes and to check the three-dimensional calculations, computational modelling was undertaken using the program Abaqus. A finite element mesh used for 3D modelling of the test geometry is shown in Figure 4.

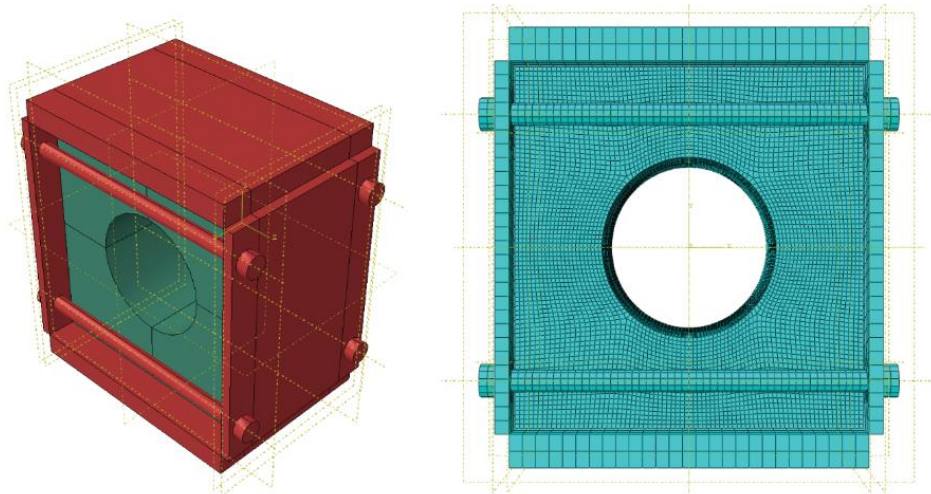


Figure 4. Three-dimensional Abaqus model geometry and finite element mesh.

3.1 Model Material Properties

For each block tested the 200mm diameter core that resulted from drilling the tunnels was subsequently re-drilled to determine the intact rock strength and elastic constants. Uniaxial Compressive Strength, σ_c and the Modulus of Elasticity E_i , were determined parallel to the vertical direction of loading. The sample specimens were prepared following the ISRM suggested methods (Brown, 1981). Two strain gauges were attached to the middle of each specimen on two opposite sides to measure the axial and lateral strains resulting from the uniaxial loadings. The results from the tests for the different rock types are shown in Figure 5. Violent failure occurred only with the strong to very strong materials.

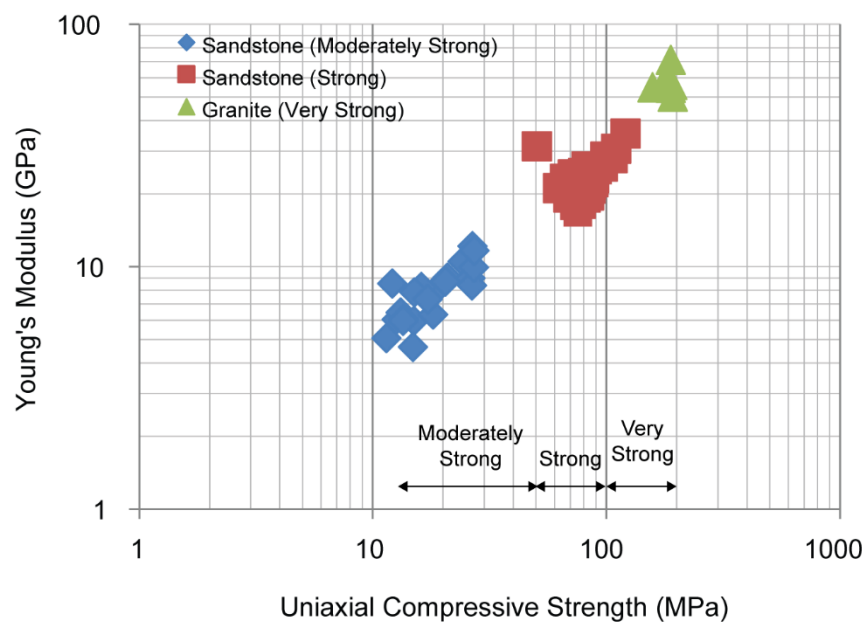


Figure 5. Intact rock strength and deformation properties for the materials tested.

In addition, triaxial testing was undertaken to obtain the cohesive strengths and friction angles at failure. Three different confining pressures ranging from 5 to 15 MPa were used during the triaxial testing. The cohesion values for the sandstone were 5 MPa and 17 MPa for moderately strong and strong material types, respectively. The granite had an average cohesion value of 25 MPa. As for the friction angle values, the moderately strong sandstone showed the lowest angle of 41°, while the strong sandstone and granite had 50° and 59° respectively.

3.2 Lateral Restraint Properties

The initial lateral stress σ_{h0} was provided by the bolt tensioning which is obtained from:

$$\sigma_{h0} = 4 \times \frac{F_0}{A} \quad (1)$$

where F_0 is the initial bolt tension force and $A (= W \times H)$ is the area of the plate.

During a test, the specimen deformed subject to the applied vertical loading. The specimens behaved elastically until spalling occurred with the lateral strain obtained by:

$$\varepsilon_h = \sigma_v \times \frac{\nu}{E} \quad (2)$$

where σ_v is the vertical loading stress, E and ν are the elastic modulus and Poisson's ratio of the rock material, respectively. The threaded bar elongations (δ) are assumed to be equal to lateral specimen deformation x . That is:

$$\delta = x = \varepsilon_h W \quad (3)$$

Then, the bolt force F_b is calculated from:

$$F_b = k \delta \quad (4)$$

where the specimen original width is W , and k is the stiffness of the bolt. The horizontal stress applied on the specimens σ_h is determined as follows.

$$\sigma_h = 4 \times \frac{F_0 + F_b}{A} \quad (5)$$

$$\sigma_h = \sigma_{h0} + 4 \frac{k\nu W}{AE} \sigma_v \quad (6)$$

3.3 Summary of Properties Used for Computational Modelling

Table 1 shows the physical properties of the rock and steel materials as used for numerical modelling purposes. A rubber layer was used to reduce the static friction between top and bottom platens and the rock blocks. Furthermore, a Teflon layer was used between the side platens and the rock blocks to reduce the development of vertical shear stresses as the rock block compressed vertically.

Table 1. Mechanical properties of rock samples and steel platens used for numerical modelling

	Unit density (kN/m ³)	Young's modulus (GPa)	Poisson's ratio	Cohesion (MPa)	Friction angle (°)	UCS (MPa)	UTS (MPa)
Sandstone (Mod Strong)	21.6	8	0.2	5	41	19	
Sandstone (Strong)	22.6	24	0.3	17	50	89	4.6
Granite (Very Strong)	26.0	58	0.2	25	59	182	
Steel	77	200	0.3				

Static friction between top/bottom platen and rock (rubber) 1.0
 Static friction between side platens and rock (Teflon) 0.04
 Static friction between steel and steel 0.5

3.4 Results of Computer Simulation

Figure 6 shows linear elastic finite element modelling results prior to spalling failure. Compression is shown as positive values with units of MPa. The results confirm the small level of confinement applied at the boundary of the simulated tunnels.

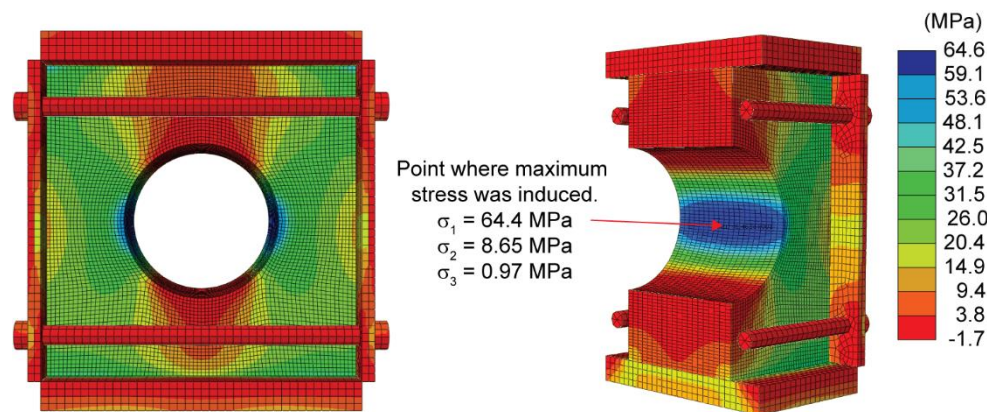


Figure 6. Maximum principal stress prior to failure.

The computational modelling solution for the maximum tangential stress (σ_{\max}) has been compared with the Kirsch solution (Hoek and Brown, 1980) and shown in Figure 7 and Table 2. Similar values of σ_c/σ_{\max} and $\sigma_c/\sigma_{\text{ave}}$ were determined by the two independent techniques.

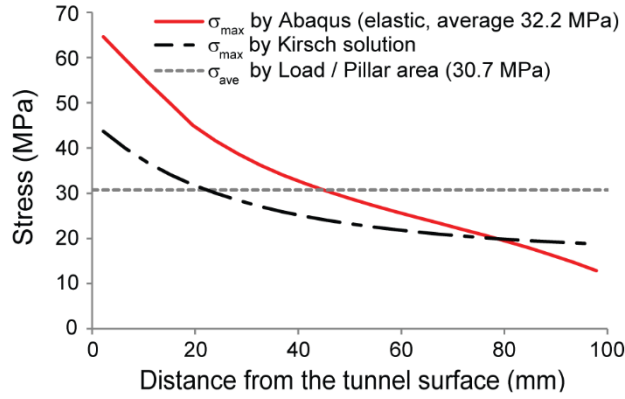


Figure 7. Calculated pillar stress distribution prior to tunnel wall spalling.

Table 2. Summary of the pillar stress prior to spalling

		Prior to spalling
Load (kN)/Vertical stress (MPa)		1124/15.3
Maximum principal stress at boundary σ_{\max} (MPa)	Abaqus Elastic	64.6
	Kirsch solution	46.0
σ_c/σ_{\max}	Abaqus Elastic	1.1
	Kirsch solution	1.6
Average pillar stress σ_{ave} (MPa)	Abaqus Elastic	32.2
	Load/Pillar area	30.7
$\sigma_c/\sigma_{\text{ave}}$	Abaqus Elastic	2.3
	Load/Pillar area	2.4

4. Testing Results

4.1 Seismic Response

For an unsupported scaled-down tunnel (and adjacent pillars) Figure 8(a) shows a typical seismic response in which loading was gradually increased from zero until tunnel wall spalling followed by pillar crushing were experienced. The seismic activity starts with the creation of a vertical tension crack in the floor and roof of the circular opening as predicted by theory (Hoek & Brown, 1980). The rate of seismic activity clearly increased prior to the violent ejection in both walls. Significantly, a relatively quiet period was monitored prior to final rupture and the start of the pillar crushing mode (shear failure) of failure. Critical levels of strength to induced stress related to the start of any visible instability such as spalling on both walls and the start of pillar have also been identified (Figure 8(b)). A significant decrease in load bearing capacity occurs following the final shear failure of the pillar.

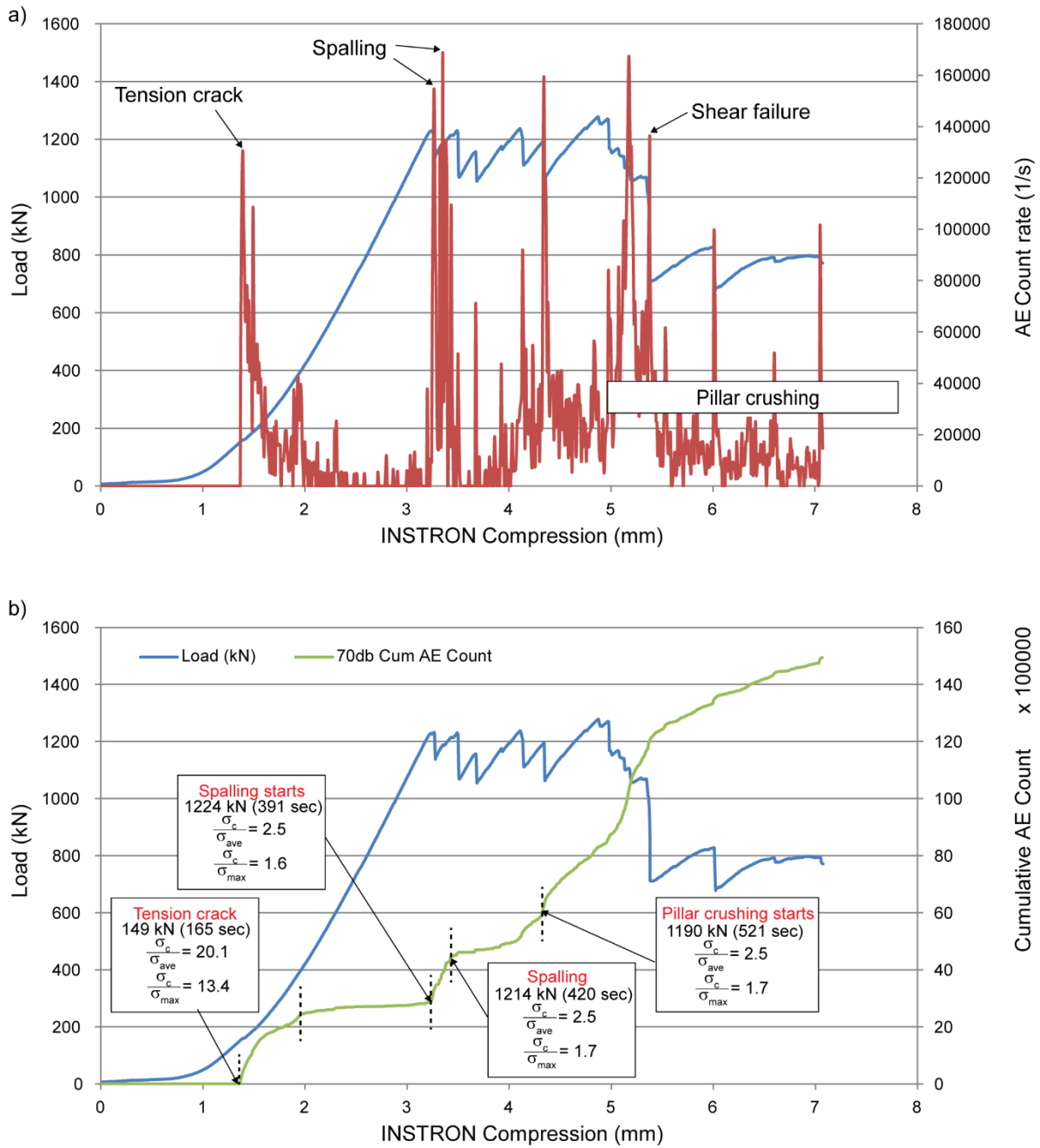


Figure 8. a) Failure mode and seismic response of an unsupported tunnel in very strong rock, b) Rate of seismicity and decreasing ratios of strength/induced stress.

4.2 Ejection Velocities

Ejection velocities ranging from 3 - 6 m/sec were determined from the experiments, which validate the back analysis of actual failures in underground mining (Ortlepp, 1993). A typical result for a wall failure is shown in Figure 9, where an ejection velocity of 5.2 m/sec can be determined using the background grid. Similar ejection velocities have been used at WASM during dynamic testing of rock reinforcement systems (Villaescusa et al., 2010). Such velocities are capable of damaging most commercially available ground support schemes.

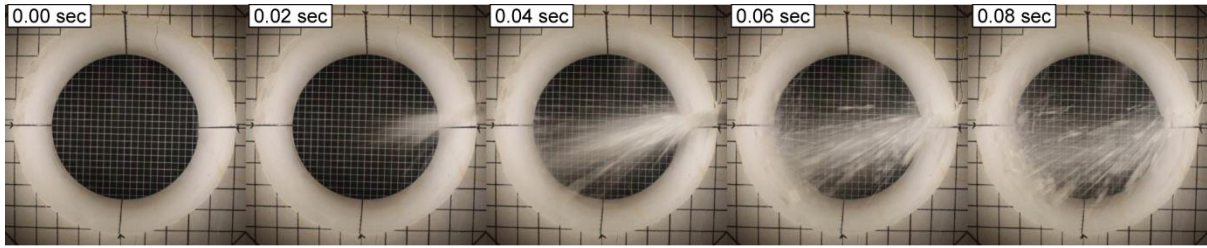


Figure 9. Determination of ejection velocity using a high speed video camera.

5. Spalling Failure

Stress-driven damage in brittle materials occurs as progressive, often violent, slabbing of the excavation walls and is localized within areas of maximum induced stress concentrations (Christiansson et al., 2012). The failure is often localized and results in an approximate v-shaped notch in the regions of violent ejection (Figure 10).



Figure 10. Notch created following stress-driven failure in a hard rock mine.

5.1 Intact Rock Strength to Induced Stress Ratios for Spalling

For the laboratory experiments described here, as the load was being increased, the ratio of compressive strength to induced stress was calculated. For immediate wall failure (spalling), the ratio monitored was the value of compressive strength to maximum tangential stress (i.e. effectively near zero confining stress at the excavation boundary). For a total of 14 laboratory tests for a range of intact rock strengths results are shown in Figure 11. The ratio of σ_c to σ_{max} was calculated using the Kirsch solution. The red dotted line and related equation represents the potential on-set of failure. i.e., the practical safe limits prior to catastrophic failure. Similar to previous work, violent ejection from the excavation walls occurred prior to peak intact rock strength (Martin et al., 1997). Significantly, the tunnels in moderately

strong rock (having a compressive strength below 50 MPa) did not experience the spalling failure mode.

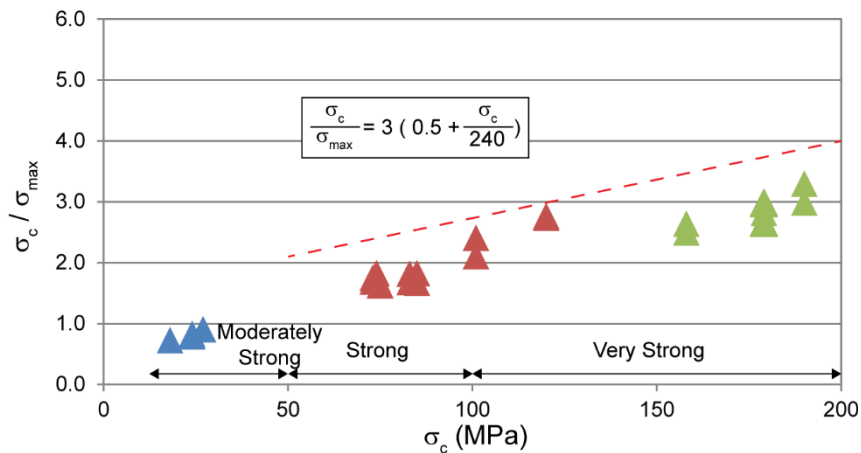


Figure 11. Unsupported tunnel spalling as a function of compressive strength and maximum tangential stress.

5.2 Comparison of Model Results with Field Observations of Spalling

The laboratory results correlate well with observations of 4 - 5m diameter full scale unsupported tunnels excavated within a rock mass having a Uniaxial Compressive Strength of 250 - 270 MPa and widely spaced tightly healed geological discontinuities. The onset of stress driven failure for the full scale unsupported tunnel was experienced for intact rock strength to maximum induced tangential stress ratio of approximately 3.5. The mining tunnels were constructed using excellent drilling and blasting techniques. The tunnels were designed with semi-circular walls and a flat floor. Incipient back (roof) failure due to a sub-horizontally oriented main principal stress component can be seen in Figure 12.



Figure 12. Full scale unsupported semi-circular tunnels showing on-set of brittle failure at the centre of the excavation roof due to high horizontal stress.

6. Pillar Crushing Failure

Pillar design and stability analysis is a critical component of a mining engineering design process. Although the fundamental concepts of Factor of Safety as the ratio of pillar strength to average pillar stress and pillar stability have been understood for some time, it is only more recently that the tools have become available to allow more quantitative analyses of pillar strength and stability to be carried out (Villaescusa, 2014).

In basic engineering mechanics terms, stability refers to the stability of equilibrium, or the ability of the overall structure, or an element of that structure such as a mine pillar, to undergo a small change in the equilibrium state of loading without producing a state of unstable equilibrium involving a sudden release of stored strain energy or large deformations (Brady and Brown, 2004). This form of instability may lead to crushing and the total collapse of a pillar and, in some cases, its surrounds. In other cases, the peak load-carrying capacity of a pillar may be exceeded and it may show visible signs of having been over-loaded, but it may retain some load-carrying capacity and continue to provide support to the mine structure without undergoing unacceptably large deformations (Villaescusa, 2014).

6.1 Intact Rock Strength to Induced Stress Ratios for Pillar Crushing

For the laboratory experiment described here, the ratio of intact rock compressive strength to the average pillar stress adjacent to the tunnels walls was calculated during loading. Figure 13 shows the results for the onset of pillar crushing mode of failure.

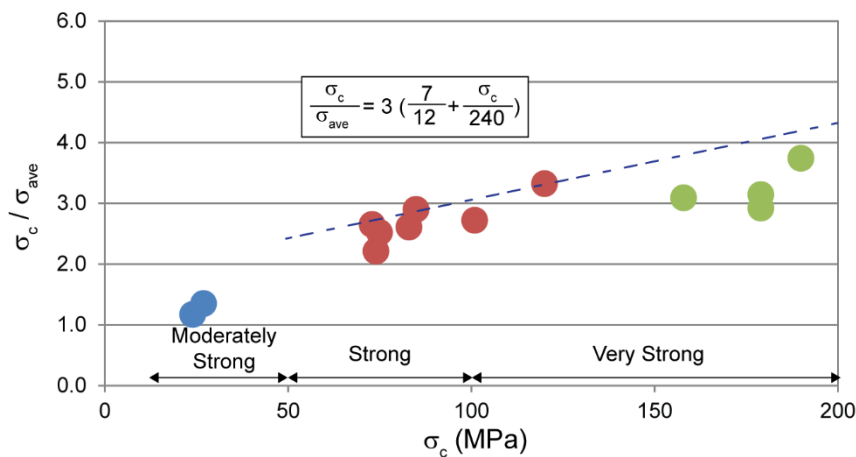


Figure 13. On-set of unsupported pillar crushing as a function of compressive strength and average pillar strength.

6.2 Non-Linear Computer Simulation

The commercial finite element code Abaqus version 6.12 was used for non-linear modelling. A Mohr-Coulomb model with a tension cut-off was adopted to describe the plastic behaviour of the specimens. During the modelling, the top platen was fixed and a constant displacement rate was applied to the bottom platen. The rate of loading during the simulation was 0.5 mm/min in an upward direction. The simulation lasted 14 minutes.

Pillar crushing was observed as steeply dipping fractures transecting the pillars which occur at higher induced stress compared with tunnel wall spalling. This can also be seen in the non-linear simulation shown in Figure 14.

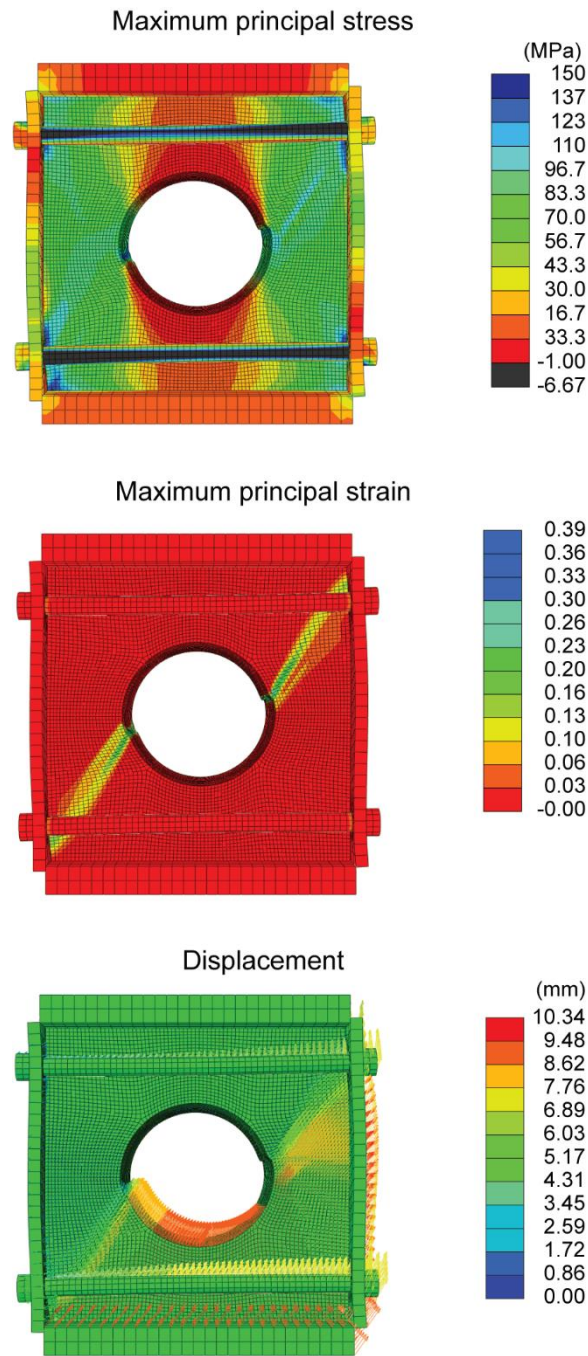


Figure 14. Modelling results of shear failure during pillar crushing using the program Abaqus.

The stress distribution in the final stages of pillar crushing can be seen in Figure 15 and are summarised in Table 3.

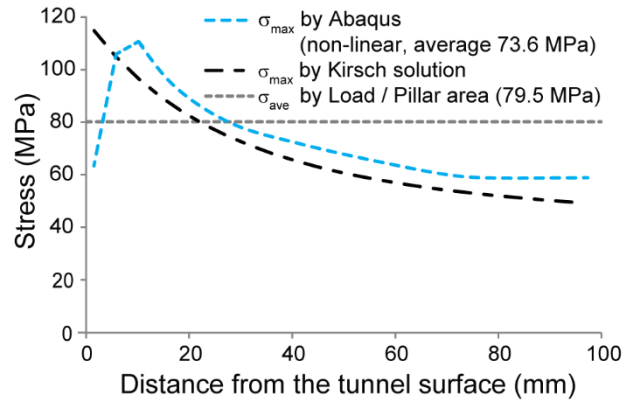


Figure 15. Determination of pillar stress distribution.

Table 3. Summary of the pillar stress prior to pillar crushing

		Prior to pillar crushing
Load (kN)/Vertical stress (MPa)		3180 / 39.8
Maximum principal stress at boundary σ_{\max} (MPa)	Abaqus Non Linear	62.7
	Kirsch solution	119.2
σ_c/σ_{\max}	Abaqus Non Linear	1.2
	Kirsch solution	0.6
Average pillar stress σ_{ave} (MPa)	Abaqus Non Linear	73.6
	Load/Pillar area	79.5
$\sigma_c/\sigma_{\text{ave}}$	Abaqus Non Linear	1.0
	Load/Pillar area	0.9

7. Application of Test Results to Pillar Design

Figure 16 shows the ratio of compressive strength to the average induced stress values experienced at pillar crushing, where shear failure was commonly experienced. The ratio of compressive strength to the average induced stress for the associated spalling failure for each pillar is also shown. As the strength of the materials decreased, the separation between spalling and pillar crushing events was less defined.

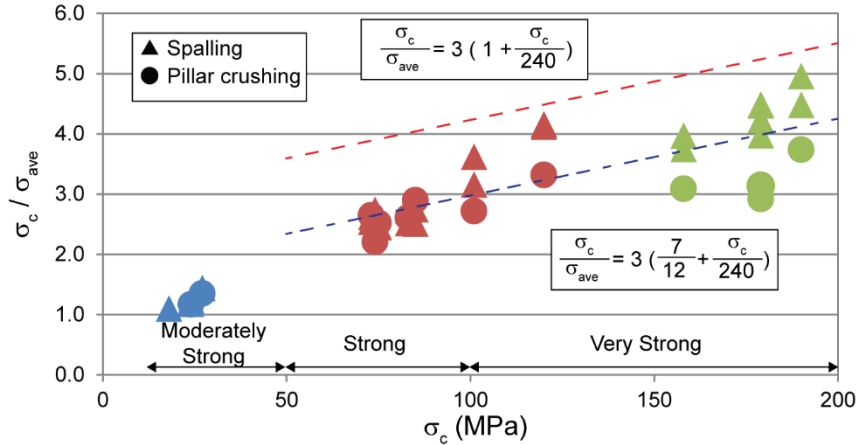


Figure 16. Progressive failure of unsupported tunnels as a function of compressive strength and average pillar strength.

7.1 Pillar Stability Graph

The results for the scaled-down unsupported pillars were compared with the full scale results from the Pillar Stability Graph database (Lunder, 1994; Villaescusa, 2014). For a range of pillar width to height (0.5 to 3.0) and the three rock types tested, the pillar crushing results from the laboratory testing compares well with the full scale results determined from underground observations (Figure 17). A slight gain on strength was detected from the laboratory samples, as they did not have any open geological structures and were tested using a slight amount of confinement. The laboratory and the field scale results suggest that for hard rock, the critical value for pillar strength is the ratio of σ_c / σ_{ave} regardless of the pillar geometry.

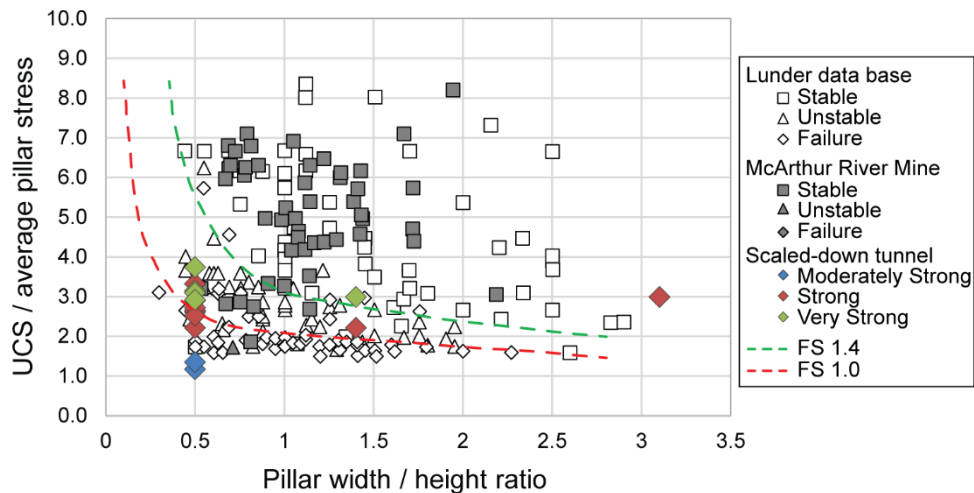


Figure 17. Comparison of scaled-down pillar crushing failure results with the full scale Pillar Stability Graph database (Villaescusa, 2014).

7.2 Failure Envelopes Derived from Model Tests

The confining pressures were modelled using non-linear finite element modelling with a typical result shown in Figure 18. In the calculations it was assumed that the

lateral stresses were caused by the reaction force of the bolt elongation as described earlier.

The low confining pressure used in the testing is representative of the confining pressure available in the vicinity of most underground excavations.

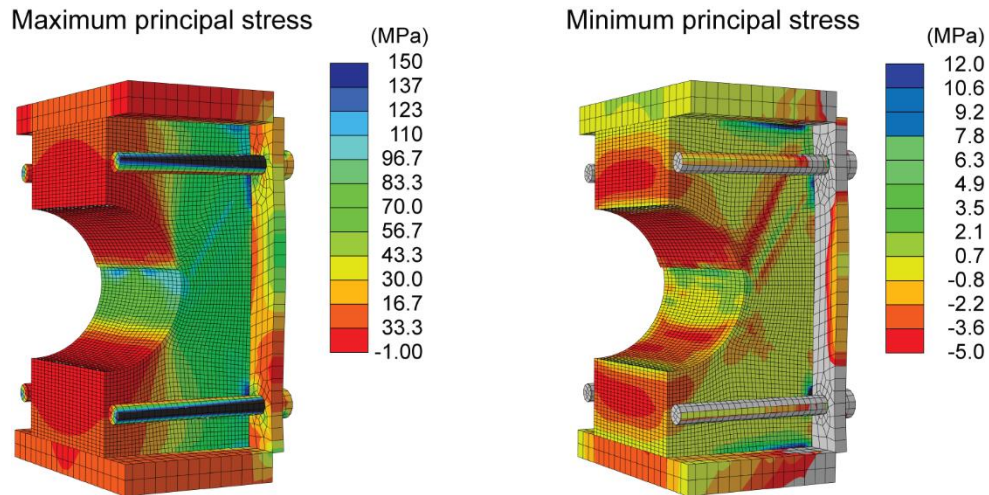


Figure 18. Section view of pillar stress distribution. Results from non-linear modelling using the program Abaqus.

Figure 19 shows the failure envelope for all the unsupported tunnel tests and the three types of materials used.

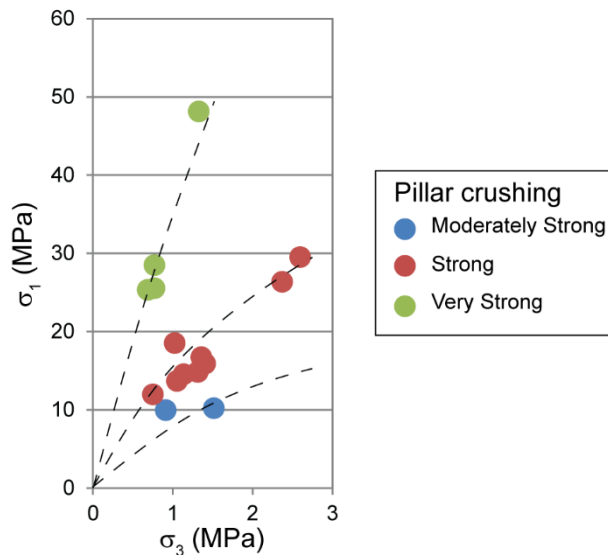


Figure 19. Failure envelopes for the scaled-down unsupported tunnels.

7.3 Strain at Spalling and Crushing

The data from the high speed video was used to calculate the strain inside the tunnels at the moment of the spalling failure. The relationships are shown in Figure

20(a). As expected, the strain at pillar crushing was slightly greater than the strain at spalling failure, as shown in Figure 20(b). The experimental results are in accordance with field data reported by Hoek (1999).

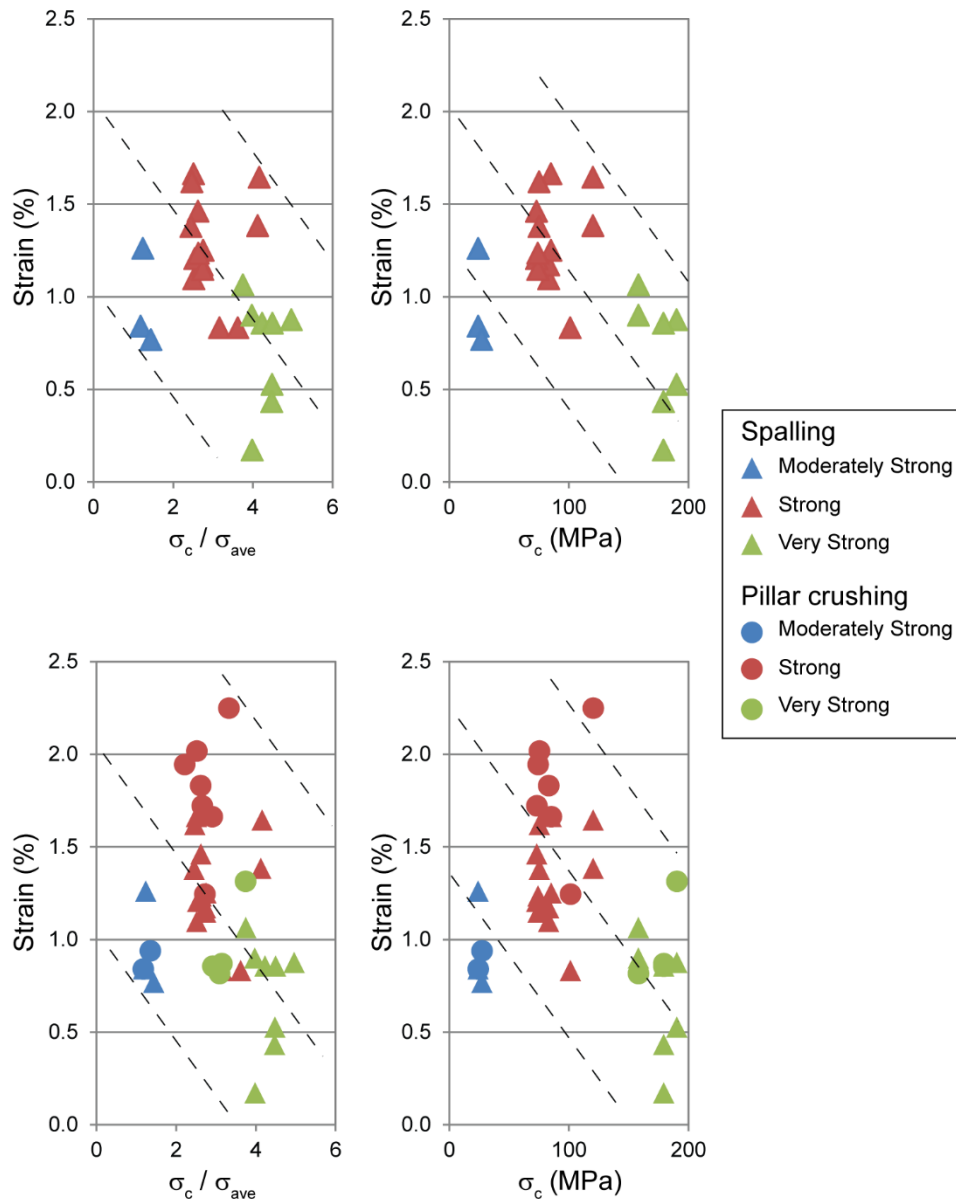


Figure 20. a) Strain at the spalling failure for the scaled-down unsupported tunnels, b) a comparison of strain at the spalling failure and pillar crushing for the scaled-down unsupported tunnels.

8. Supported Tunnels

The emphasis thus far in the paper has been to quantify the critical ratios of intact rock strength to tangential stress that result in spalling and pillar crushing around unsupported circular tunnels in different strength rocks. It is well established that ground support cannot prevent rock mass failure. However, in practice, ground

support is used in an attempt to maintain serviceability of excavations after rock mass failure. The research team have developed unique techniques to install reinforcement in boreholes drilled radially in the rock block from within the scale tunnels and materials to simulate mesh and shotcrete surface support.

The laboratory experiments also allow assessment and relative comparisons of different scaled-down ground support schemes (Figure 21). However, the behaviour of supported excavations is complex and beyond the scope of this paper and constitutes the topic of on-going research at the WASM. It is expected that the ground support will limit radial inward displacements and increase the residual crushing strength of the pillars.

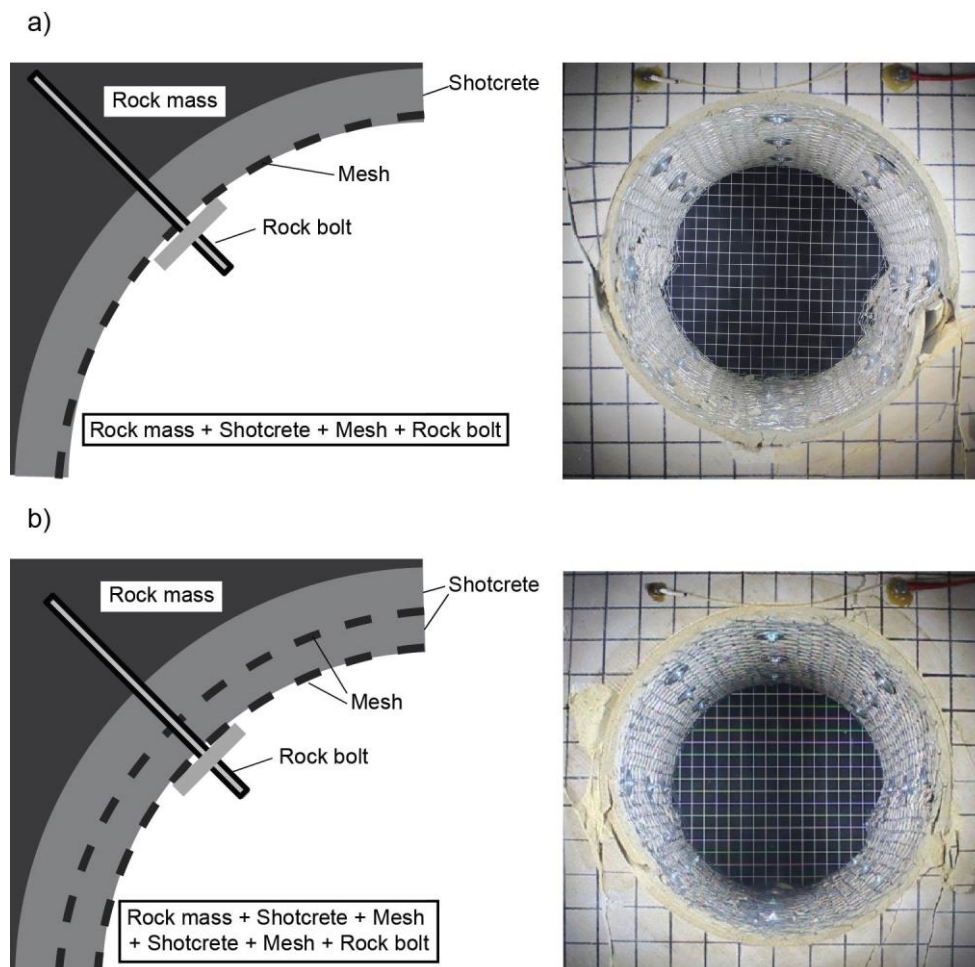


Figure 21. Comparison of ground support schemes installed within scaled-down circular tunnels.

9. Concluding Remarks

A number of empirical relationships have been determined for the onset of spalling and pillar crushing for scaled-down tunnels drilled into three different material types. The data suggest that a distinctive ratio of compressive strength to induced stress can be determined for the different stages of progressive failure (i.e., spalling at the tunnel boundaries and pillar crushing adjacent to the tunnels). The relationship

appears to be linear and a function of the compressive strength of the materials. The results from laboratory scale tests compare well with data from full scale excavations from a number of mine pillars suggesting that the ratios of compressive strength to induced stress that trigger the onset of spalling and pillar crushing are scale independent. Furthermore, ejection velocities determined from the scaled-down experiments are in a similar range to those back calculated from full scale underground failures.

Acknowledgements

The authors wish to acknowledge the invaluable expertise and assistance provided by Prof. E. T. Brown, Dr. Alan Thompson, Pat Hogan and Lance Fraser. Their help during sample preparation, testing, data analysis and paper writing is greatly acknowledged.

References

- Barla, G. 2014. TBM tunnelling in deep underground excavation in hard rock with spalling behaviour. Proceedings of the 43rd Geomechanics Colloquium, Freiberg:25-39.
- Barton, N., Lein, R., and Lunde, J. 1974. Engineering classification of rock masses for design of tunnel support. Rock Mechanics, 6(4): 189-236.
- Brady, B.H.G. and Brown, E.T. 2004. Rock mechanics for underground mining, 3rd Edition, 628pp. Dordrecht, The Netherlands:Kluwer.
- Brown, E.T. 1981. Rock characterization, testing & monitoring: ISRM suggested methods. Published for the Commission on Testing Methods, International Society for Rock Mechanics by Pergamon Press, Oxford
- Christiansson, R. Hakala, M. Kempainen, K. Siren, T. and Martin, C.D. 2012. Findings from large scale in-situ experiments to establish the initiation of spalling. Eurock, 12p.
- Hoek, E., Brown, E. T. 1980. Underground excavations in rock. London, Institution of Mining and Metallurgy, London, 527 pp.
- Hoek, E. 1999. Support for very weak rock associated with faults and shear zones. Rock Support and Reinforcement Practice in Mining (Ed. Villaescusa, E., Windsor, C.R. and Thompson, A.), 19-30pp. Balkema, Rotterdam.
- Hutchinson, D. J. and Diederichs, M. S. 1996. Cablebolting in Underground Mines, 406pp. Richmond, British Columbia, Canada: Bitech Publishers.
- Lunder, P. 1994. Hard rock pillar strength estimation: An applied empirical approach. MASC thesis, University of British Columbia, Vancouver, British Columbia, Canada, 166pp.
- Martin, C.D. Read, R.S. and Martino, J.B. 1997. Observations of brittle failure around a circular test tunnel. International Journal of Rock Mechanics and Mining Sciences, 34(7): 1065-1073.
- Mathews, K. E., Hoek, E., Wyllie, D. C., and Stewart, S. B. V. 1980. Prediction of stable excavation spans for mining at depths below 1,000 Metres in hard rock. Ottawa,

Ontario, Canada: Golder Associates Report to Canada Centre for Mining and Energy Technology (CANMET), Department of Energy and Resources.

Ortlepp, W.D., 1993. High Ground Displacement Velocities Associated with Rockburst Damage. *Rockbursts and Seismicity in Mines* 93: 101-106.

Villaescusa, E., Thompson, A., Player, J. and Morton, E. 2010. Dynamic Testing of Ground Control. Report No. 287, Minerals and Energy Research Institute of Western Australia, 187pp.

Villaescusa, E. 2014. Geotechnical Design for Sublevel Stopping, CRC Press, 519pp.